TECHNICAL ARTICLE

Phase relation, structure, and properties of borate $MgYB_5O_{10}$ in $MgO–Y_2O_3–B_2O_3$ system

Jing Zhang,[1,2] Xiaoma Tao,[3] Gemei Cai,[1,2,a)] and Zhanpeng Jin[1,2]
[1]School of Materials Science and Engineering, Central South University, Changsha, Hunan 410083, China
[2]Education Ministry Key Laboratory of Non-ferrous Materials Science and Engineering, Central South University, Changsha 410083, China
[3]College of Physical Science and Technology, Guangxi University, Nanning 530004, China

(Received 8 September 2016; accepted 26 January 2017)

In the investigation of $MgO–Y_2O_3–B_2O_3$ system, six three-phase regions, five binary compounds, and one ternary compound $MgYB_5O_{10}$ were confirmed in the subsolidus phase relations. Single-phase powder sample of $MgYB_5O_{10}$ was successfully prepared through solution synthesis method. By using the Rietveld method from the step-scanning X-ray powder diffraction data, the crystal structure of $MgYB_5O_{10}$ was determined. It crystallizes in the monoclinic system with the space group $P12_1/c1$ and lattice parameters $a = 8.5113(2)$ Å, $b = 7.5892(2)$ Å, $c = 12.2460(3)$ Å, $\beta = 130.200(1)°$, and $Z = 4$. The infrared spectrum of $MgYB_5O_{10}$ at room temperature demonstrates the existence of BO_3 and BO_4 groups. The UV–visible spectrum shows a wide absorption band within the range of 190–400 nm, while the absorption in the visible region is negligible. According to the electronic structure derived by first-principles calculations, $MgYB_5O_{10}$ is an insulator with a wide indirect energy band gap of about 5.95 eV. Layered structural characteristics, existence of one-dimensional Y_nO_{8n+2} chains, and the large band gap should be the immanent reason why $MgYB_5O_{10}$-based materials have exhibited outstanding performances in the luminescence field. © *2017 International Centre for Diffraction Data*. [doi:10.1017/S0885715617000227]

Key words: borate, $MgYB_5O_{10}$, crystal structure, electronic structure, band gap

I. INTRODUCTION

Borates, which usually feature diverse structure, high laser damage tolerance, wide transparency spectra range, good stability, and interesting thermal expansion, have shown their merit as functional materials (Chen *et al.*, 1990; Becker, 1998; Sasaki *et al.*, 2000; Lou *et al.*, 2015; Jiang *et al.*, 2016). In the past decades, a number of borates with superior optical properties have been synthesized and put into various applications. For example, $K_2Al_2B_2O_7$ (KAB) (Hu *et al.*, 1998), β-BaB_2O_4 (BBO) (Bosenberg *et al.*, 1989), LiB_3O_5 (LBO) (Kellner *et al.*, 1997), and $Se_2B_2O_7$ (SBO) (Kong *et al.*, 2006) have been used for second harmonic generation; YBO_3 (Wei *et al.*, 2002), $Ba_2Mg(BO_3)_2$ (Hu *et al.*, 2015), $Na_3Gd(BO_3)_2$ (Shi *et al.*, 2016), and $K_3YB_6O_{12}$ (Yang *et al.*, 2016) are desirable hosts of phosphor; and $Ba_3InB_9O_{18}$ shows to be promising candidate for efficient scintillators used for X-ray detection applications (Cai *et al.*, 2008).

As is known from the preceding study, lots of compounds with unique and outstanding properties have been generated from ternary borates of alkaline metals and rare earths. Saubat *et al.* (1980) systematically investigated lanthanide magnesium pentaborates $MgLnB_5O_{10}$ (Ln = La, Ce, Pr, Nd, Sm, Eu, Gd, Tb, Dy, Ho, and Er). As a category of boron-rich borates, $MgLnB_5O_{10}$ compounds crystallize in a monoclinic structure belonging to space group $P12_1/c1$, and have turned out to be favorable solid-state laser materials and phosphors hosts. Nd^{3+}-doped $MgGd(BO_2)_5$ has been characterized by a very strong absorption at near 808 nm and intense emission as a potential diode-pumped laser crystal (Fan *et al.*, 2006), while Yb^{3+}, Mn^{2+}-codoped $MgGdB_5O_{10}$ has been demonstrated to generate room-temperature up-converted white light under the excitation of 976 nm diode laser (Ye *et al.*, 2011). Notably, previous studies have focused on the properties especially luminescence performances of rear earth-doped $MgYB_5O_{10}$. Knitel *et al.* reported the photoluminescence properties of $MgYB_5O_{10}$: Ce^{3+}, which generates a broad self-trapped exciton (STE) emission band under X-ray excitation (Knitel *et al.*, 2000). However, they failed to obtain single-phase samples by neither changing the amount of excessive H_3BO_3 nor prolonging the firing time. In addition, Zhou *et al.* (2007) studied the luminescence properties of $MO–Re_2O_3–B_2O_3$:Eu^{3+} (M = Mg, Sr; Re = Y, Gd) under vacuum ultraviolet (VUV) excitation, which included the ternary system we paid attention to in this work. Anyhow, it can be seen from the X-ray pattern given in their paper that the sample of $MgYB_5O_{10}$ was also not pure in their work. Moreover, little research has paid attention to the phase relations of the $MgO–Y_2O_3–B_2O_3$ ternary system.

Therefore, in the present work, the subsolidus phase relations of $MgO–Y_2O_3–B_2O_3$ ternary system were investigated, in which only one ternary compound, $MgYB_5O_{10}$, was confirmed. Single-phase powder sample of $MgYB_5O_{10}$ was successfully obtained by the solution method. Although

a)Author to whom correspondence should be addressed. Electronic mail: caigemei@csu.edu.cn

Peterson (1999) has studied $MgYB_5O_{10}$ and solved the structure by single-crystal diffraction method, the obtained results is in non-standard space group $P12_1/n$. Thus, we re-investigated it by the powder X-ray diffraction (XRD) and Rietveld method in this work. For the first time, first-principles calculations on the electronic structure of $MgYB_5O_{10}$ at $T = 0$ K have been performed in order for a better understanding of its basic physical properties.

II. EXPERIMENTAL

Samples were synthesized by the high-temperature solid-state reaction method when we explored the subsolidus phase relation of the MgO–Y_2O_3–B_2O_3 ternary system. Stoichiometric mixtures of MgO (spectral reagent), Y_2O_3 (analytical reagent), and H_3BO_3 (analytical reagent) were ground into homogeneous powders in an agate mortar and then were preheated in corundum crucibles for 12 h at 400–600 °C. The preheating process is to decompose H_3BO_3 and some other impurities. After cooling down to room temperature in the furnace, the mixtures were reground and calcined at 800–1100 °C for 24–48 h depending on their compositions. Finally, all the samples were naturally cooled to room temperature. In all cases, an excess amount (~2 at.%) of H_3BO_3 was added in order to compensate the losses of B_2O_3 in the heating processes. Especially, single-phase $MgYB_5O_{10}$ sample was synthesized by the Pechini method as following: stoichiometric mixtures were dissolved into dilute nitric acid and then some amount of polyvinyl alcohol was added as a complexing agent. The solution was heated with stirring to evaporate water and obtain a porous gel. Subsequently, the gel was ground and calcined at 700 °C for 48 h.

Powder XRD patterns were collected by Rigaku diffractometer D/MAX-2500 with Cu$K\alpha$ radiation and graphite monochromator operated at 40 kV, 150 mA. The powder XRD data for crystal structure analyses were collected at room temperature under the step-scanning mode with a step size of 0.02° (2θ), counting time of 2 s step^{-1} and 2θ ranges of 10°–130°. Inorganic Crystal Structure Database (ICSD) and Powder Diffraction File (PDF-4 + 2011) were used for the phase analyses.

Infrared (IR) spectroscopy measurement was conducted with the objective of specifying and comparing the coordination of boron in $MgYB_5O_{10}$. The mid-IR spectrum ranging from 400 to 2000 cm^{-1} was obtained at room temperature via a Perkin–Elmer 983 G IR spectrophotometer with KBr pellets as standards.

The UV–visible (UV–vis) diffuse reflectance spectrum was measured through an SHIMADZU/UV-2450 UV spectrophotometer in the wavelength range from 200 to 700 nm.

First-principles calculations of the electronic structure for $MgYB_5O_{10}$ were performed using the scalar relativistic all-electron Bloch's projector augmented wave method within the generalized gradient approximation (GGA), as implemented in the highly efficient Vienna *ab initio* simulation package. For the GGA exchange-correlation potential, the Perdew–Burke–Ernzerhof parameterization was employed. The *k*-point meshes for Brillouin zone sampling were constructed using the Monkhorst–Pack scheme, and the reciprocal space meshes were increased to achieve convergence to a precision of better than 1 meV at^{-1}. The plane-wave kinetic-energy cutoff was set as 600 eV for all calculations. The structure was optimized by minimization of the forces acting on the atoms. When the forces were minimized in this construction, one could then find the self-consistent density at these positions via turning off the relaxations and driving the system to self-consistency. We took the full relativistic effects for core states and used the scalar relativistic approximation for the valence states.

III. RESULTS AND DISCUSSION

A. Subsolidus phase relations in MgO–Y_2O_3–B_2O_3 system

In the binary system MgO–B_2O_3, four binary compounds MgB_2O_4, $Mg_3B_2O_6$ [ICSD #31385], $Mg_2B_2O_5$ [ICSD #79721], and MgB_4O_7 [ICSD #34397] (Sadanaga, 1948; Kuzel, 1964; Bartl and Schuckmann, 1966; Guo *et al.,* 1995) have been reported in former study. All of them but the first were confirmed in the present work. Mutluer and Timucin (1975) verified the "compound" MgB_2O_4's absence through the XRD pattern, DTA, and petrographic evidence, which agrees with the observation of some other researchers' work (Kuzel, 1964; Fletcher *et al.,* 1970; Bazarova *et al.,* 2007). This is identical with our experimental results. In addition, it is suggested that the considered MgB_2O_4 is mixture of MgB_4O_7 and $Mg_2B_2O_5$.

In the Y_2O_3–B_2O_3 binary system, two binary compounds YBO_3 [ICSD #27931] and Y_3BO_6 [ICDD–PDF 34-0291] (Levin *et al.,* 1961; Chadeyron *et al.,* 1997) were reported to exist, which is in coherence with our work.

As for the binary system MgO–Y_2O_3, there is no binary compound, which is in coincidence with both the results of literature research and our experiment.

Based on the phase identifications of nine samples with different compositions as listed in Table I, subsolidus phase

TABLE I. List of phase identification in the system MgO–Y_2O_3–B_2O_3.

Samples	MgO (at.%)	$YO_{1.5}$ (at.%)	$BO_{1.5}$ (at.%)	Synthesis temperature (°C)	Phase composition
1	20	70	10	1200	$Y_3BO_6 + Y_2O_3 + MgO$
2	65	10	25	1100	$YBO_3 + Mg_3B_2O_6 + MgO$
3	15	50	35	1100	$YBO_3 + Y_3BO_6 + MgO$
4	10	10	80	800	$YBO_3 + MgB_4O_7 + M$
5	25	5	70	850	$YBO_3 + Mg_2B_2O_5 + MgB_4O_7$
6	45	8	47	1000	$YBO_3 + Mg_2B_2O_5 + Mg_3B_2O_6$
7	33.3	33.3	33.4	1200	$MgO + Y_3BO_6 + YBO_3$
8	50	12.5	37.5	1200	$YBO_3 + Mg_3B_2O_6 + MgO$
M	14.3	14.3	71.4	900	$YBO_3 + MgB_4O_7 + M$

https://doi.org/10.1017/S0885715617000227 Published online by Cambridge University Press

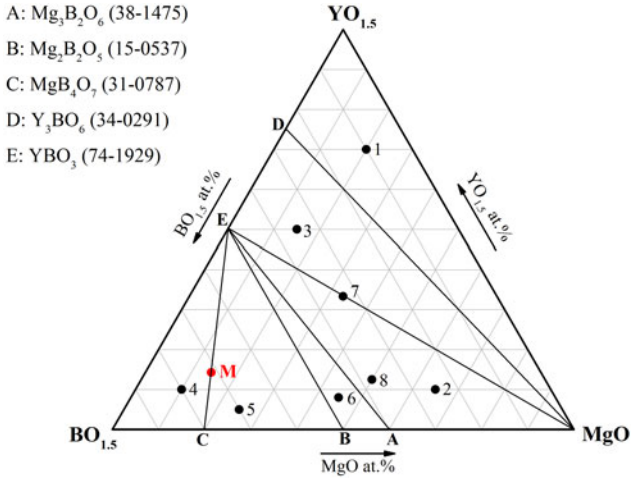

Figure 1. Subsolidus phase relations in the system MgO–Y_2O_3–B_2O_3.

relations of MgO–Y_2O_3–B_2O_3 ternary system were determined under present experimental conditions, as shown in Figure 1. There are six definite three-phase regions and no unanimous solution exists. Only one ternary compound $MgYB_5O_{10}$ was found in this system. In this work, pure $MgYB_5O_{10}$ powder sample was successfully obtained by the Pechini method, which effectively suppressed the formation of YBO_3 impurities.

B. Crystal structure of $MgYB_5O_{10}$

Using the program DICVOL04 (Boultif and Louër, 2004) by the successive dichotomy method, all the reflections ($2\theta \leq 50°$) of the compound $MgYB_5O_{10}$ can be well indexed on the basis of a monoclinic unit cell with lattice parameters $a = 8.5084$ Å, $b = 7.5843$ Å, $c = 9.3689$ Å, $\beta = 93.740°$, with $F(20) = 77.0$ and $M(20) = 40.3$. Table II shows the detail information of indexing result for compound $MgYB_5O_{10}$. According to the reflecting conditions, we can make a conclusion that $MgYB_5O_{10}$ crystallizes in the space group of $P12_1/n1$ (non-standard). The non-standard space group was transformed into standard form $P12_1/c1$ with crystal parameters $a = 8.5084$ Å, $b = 7.5843$ Å, $c = 12.2346$ Å, and $\beta = 130.142°$. According to comparisons between $MgYB_5O_{10}$ and $ZnLaB_5O_{10}$ (Jiao *et al.,* 2010) in the crystal system, $MgYB_5O_{10}$ and $ZnLaB_5O_{10}$ are isostructural.

Thus, taking $ZnLaB_5O_{10}$ (Jiao *et al.,* 2010) as the preliminary crystal structure model, the structure parameters of $MgYB_5O_{10}$ was refined and re-determined in this work. The process was accomplished by the Rietveld method (Rietveld, 1967) using the program FullProf_suite. In the structure refinement, we used the diffraction data in the range of $2\theta =$ 10–130° and chose Pseudo-Voigt function as peak shape function. Consequently, 75 parameters were refined in all, including 63 structure parameters and 12 profile parameters. In this structure, all atoms are located on the crystal lattice position 4*e*, which is similar to that of $ZnLaB_5O_{10}$. The agreement factors in the structure refinement were finally converged to $R_B = 3.84\%$, $R_P = 2.55\%$, $R_{WP} = 3.20\%$, and $S = 1.86$, which indicates the structure model is quite receivable. More details of refinement data are listed in Table III. Figure 2 is the final refinement pattern. Observed intensities are represented by the red hollow circle, the calculated intensities by the black line, and the difference plot by the blue line. The positions of all Bragg reflections are marked with the green bars. Refined structural parameters, including atomic coordinates, Wyckoff positions and isotropic displacement parameters are listed in Table IV. Asymmetric unit of $MgYB_5O_{10}$ comprises of one unique Mg atom, one unique Y atom, five unique B atoms, and ten unique O atoms. Figures 3(a), 3(b), and 3(c) are the projection view of the crystal structure of $MgYB_5O_{10}$ along *a, b*, and *c*-axes, respectively. Three of the B atoms are coordinated with four O atoms to form tetrahedron BO_4 units and the other two B

TABLE II. Details of indexing result for the compound $MgYB_5O_{10}$.

h	*k*	*l*	d_{obs}	d_{cal}	$2\theta_{obs}$	$2\theta_{cal}$	$\Delta 2\theta$	I_{obs}
1	0	−1	6.5242	6.5260	13.561	13.557	0.004	834
1	0	1	6.1153	6.1160	14.473	14.471	0.002	740
0	1	1	5.6777	5.6771	15.595	15.597	−0.002	144
1	1	1	4.7605	4.7642	18.624	18.609	0.015	144
2	0	0	4.6893	4.6902	18.909	18.906	0.004	528
0	0	2	4.2565	4.2541	20.853	20.864	−0.012	122
0	2	0	3.8009	3.8021	23.386	23.378	0.008	96
0	1	2	3.7130	3.7114	23.947	23.958	−0.011	1000
1	1	−2	3.5217	3.5225	25.269	25.263	−0.006	281
0	2	1	3.4711	3.4702	25.644	25.650	−0.007	142
1	1	2	3.3856	3.3850	26.302	26.308	−0.005	141
1	2	−1	3.2820	3.2822	27.148	27.147	0.001	789
2	0	−2	3.2565	3.2548	27.365	27.380	−0.015	532
1	2	1	3.2267	3.2260	27.623	27.629	−0.007	629
2	0	2	3.0506	3.0508	29.252	29.250	0.002	17
2	1	−2	2.9942	2.9946	29.816	29.812	0.004	296
2	2	0	2.9504	2.9508	30.268	30.265	0.003	277
3	0	1	2.8715	2.8713	31.121	31.124	−0.003	463
0	0	3	2.8305	2.8307	31.584	31.581	0.003	972
1	0	−3	2.7597	2.7615	32.416	32.394	0.022	327

TABLE III. Details of Rietveld refinement and crystal data for the structure $MgYB_5O_{10}$.

Sample	Multi-crystal powder
Diffractometer	Rigaku D/MAX-2500
Radiation type	Cu *K*α
Monochromator	Graphite
Wavelength (Å) for Ka1	1.5406
Refined Profile range 2θ (°)	10–130
Step size 2θ (°)	0.02
Step scan time per step (s)	2
Number of structure parameters	63
Number of profile parameters	12
R_B	3.84%
R_P	2.55%
R_{WP}	3.20%
S	1.86
Formula	$MgYB_5O_{10}$
Symmetry	Monoclinic
Space group	$P12_1/c1$
a (Å)	8.5113(2)
b (Å)	7.5892(2)
c (Å)	12.2460(3)
β (°)	130.200(1)
V (Å^3)	604.18(2)
Z	4
Calculated density (g cm^{-3})	3.5976

https://doi.org/10.1017/S0885715617000227 Published online by Cambridge University Press

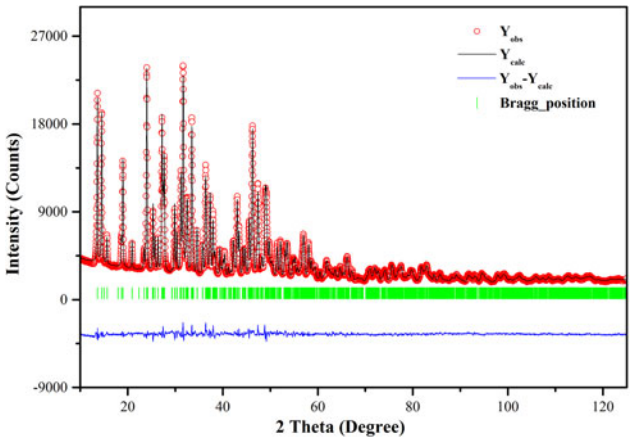

Figure 2. The final Rietveld refinement pattern for $MgYB_5O_{10}$.

atoms are three-coordinated and build triangular BO_3 units. As shown in Figure 3(d), jointed by BO_4 in the middle, three BO_4 units, and two BO_3 units can be connected to form a B_5O_{12} double-ring complex group. Double-ring B_5O_{12} can further assemble infinite two-dimensional (2D) layers $[B_5O_{10}]_n^{5-}$ via corner-sharing O atom between two adjacent B_5O_{12} groups [Figure 3(b)]. Countless $[B_5O_{10}]_n^{5-}$ layers are linked together by Mg and Y atoms forming the fundamental framework of $MgYB_5O_{10}$, which are perpendicular to the *ac*-crystallographic plane.

The Mg atoms are surrounded by six O atoms to make up the MgO_6 octahedra. From the view along *a*-axis direction, two adjacent MgO_6 octahedra form an isolated Mg_2O_{10} group through sharing an edge [Figures 3(a) and 3(e)]. The Y atoms are connected with ten atoms to form distortional YO_{10} polyhedra. Edge-sharing YO_{10} polyhedra can form infinite zigzag Y_nO_{8n+2} chains stretching along *b*-axis (Figure 3(f)).

In the structure, the average lengths of the B–O bond in BO_3 and BO_4 groups are 1.35 and 1.48 Å, respectively, which are close to those observed in other known borates (Busche and Bluhm, 1996; Chen *et al.,* 2007; Jiao *et al.,* 2010). The Mg–O bond lengths are in the range of 1.987–2.297 Å (2.11 Å in average) and the Y–O bond lengths are in the range of 2.291–2.890 Å (2.53 Å in average). Representative bond lengths, angles, and coordination number (CN) of cations are given in Table V. These values are approximately consistent with the corresponding bond lengths or angles found in other magnesium borates (Yang *et al.,* 2001; Li *et al.,* 2013) and yttrium borates (Chadeyron *et al.,* 1997; Li *et al.*, 2004). The shortest distances of Y–Y in $MgYB_5O_{10}$ are 3.953 and 6.007 Å for intrachain and interchain, respectively. The process of intrachain energy transfer is much easier than that of interchain. In addition, 1D energy transfer can depress the backward energy migration to some extent, which further improved the transmission efficiency (Hong, 2011). Short distance may result in strong interaction of energy levels of active ions, which occupy the Y sites when $MgYB_5O_{10}$ is doped, probably leading to strong fluorescence concentration quenching and short fluorescence lifetime.

In order to examine the rationality of the determined structure of $MgYB_5O_{10}$, Brown's bond valence method (Brown and Altermatt, 1985) was utilized to calculate the valence sum for each ion. From the results given in Table VI, the bond valence sum of each cation is in very good agreement with the formal oxidation state, indicating that the calculated valence sums for all ions are reasonable in this structure.

TABLE IV. Atomic coordinates and isotropic displacement for $MgYB_5O_{10}$.

Atom	Site	*x*	*y*	*z*	B(Å^2)
Y	4*e*	0.0535(1)	0.8145(1)	0.2388(1)	0.825(3)
Mg	4*e*	0.4701(2)	0.0955(2)	0.3714(2)	0.336(8)
O(1)	4*e*	0.2008(2)	0.2892(2)	0.2323(1)	0.193(4)
O(2)	4*e*	0.6856(2)	0.0906(1)	0.1964(1)	0.193(4)
O(3)	4*e*	0.3108(2)	0.4630(1)	0.1242(1)	0.193(4)
O(4)	4*e*	0.2348(2)	0.0275(2)	0.1498(1)	0.193(4)
O(5)	4*e*	0.0960(2)	0.6130(1)	0.4202(1)	0.193(4)
O(6)	4*e*	0.0267(2)	0.2284(2)	0.4816(1)	0.193(4)
O(7)	4*e*	0.5477(2)	0.3463(2)	0.3655(1)	0.193(4)
O(8)	4*e*	0.3375(2)	0.1258(2)	0.0156(1)	0.193(4)
O(9)	4*e*	0.5721(2)	0.3539(2)	0.0669(1)	0.193(4)
O(10)	4*e*	0.1287(2)	0.0528(2)	0.3802(1)	0.193(4)
B(1)	4*e*	0.3589(2)	0.4386(2)	0.2657(1)	0.451(12)
B(2)	4*e*	0.5358(2)	0.1946(2)	0.0965(1)	0.451(12)
B(3)	4*e*	0.0959(2)	0.1740(2)	0.1084(1)	0.451(12)
B(4)	4*e*	0.2984(2)	0.5329(2)	0.5698(1)	0.451(12)
B(5)	4*e*	0.1528(2)	0.4052(1)	−0.0006(1)	0.451(12)

C. IR spectra of $MgYB_5O_{10}$

To further confirm the coordination surroundings of boron in the $MgYB_5O_{10}$, the IR absorption spectrum was measured at room temperature, which is shown in Figure 4. All the experimental peak positions of $MgYB_5O_{10}$ along with their assignments are displayed in Table VII, in which the reported data of $Na_3ZnB_5O_{10}$ (Chen *et al.,* 2012) are also given for comparison. The absorption wavenumber profile in 1300–1500 cm^{-1} should be assigned to the asymmetric stretching vibrations (ν_{as}) of BO_3 groups. Strong bands observed at 1000–1200 cm^{-1} should be attributed to asymmetric stretching vibrations (ν_{as}) of BO_4 groups. Those peaks at 800–1000 cm^{-1} should be the characteristic symmetric stretching of BO_3 groups. The bands located at about 680–800 cm^{-1} can be assigned to the symmetric stretching vibrations (ν_s) of BO_4 and symmetric bending (γ) of BO_3 groups, while the absorption below 680 cm^{-1} wavenumber mainly originates from the symmetric bending (γ) and asymmetric bending (δ) of BO_3 and BO_4 groups. IR spectrum of $MgYB_5O_{10}$ certifies the presence of BO_3 and BO_4 groups in the structure.

D. Crystal structure of compounds MRB_5O_{10}

Most of the pentaborate family with the formula MRB_5O_{10} (*M* and *R* are divalent and trivalent cations, respectively) reported in previous literatures are isostructural and crystallize in the $P12_1/c1$ (No. 14) space group, expect for the small brunches with the formula $CuRB_5O_{10}$, which belong to the orthorhombic crystal system. Table VIII lists the space group, CN of *M* and *R* ions, and lattice parameters (*a, b, c*, and β) of MRB_5O_{10} compounds reported in both previous literatures and this work. It was found that all *M* ions have sixfold coordination. But the CN of *R* ions differs when compounds are in different space group. For those monoclinic compounds, the fundamental structure of anion group has the double-ring configuration, which is constructed by three BO_4 tetrahedra

https://doi.org/10.1017/S0885715617000227 Published online by Cambridge University Press

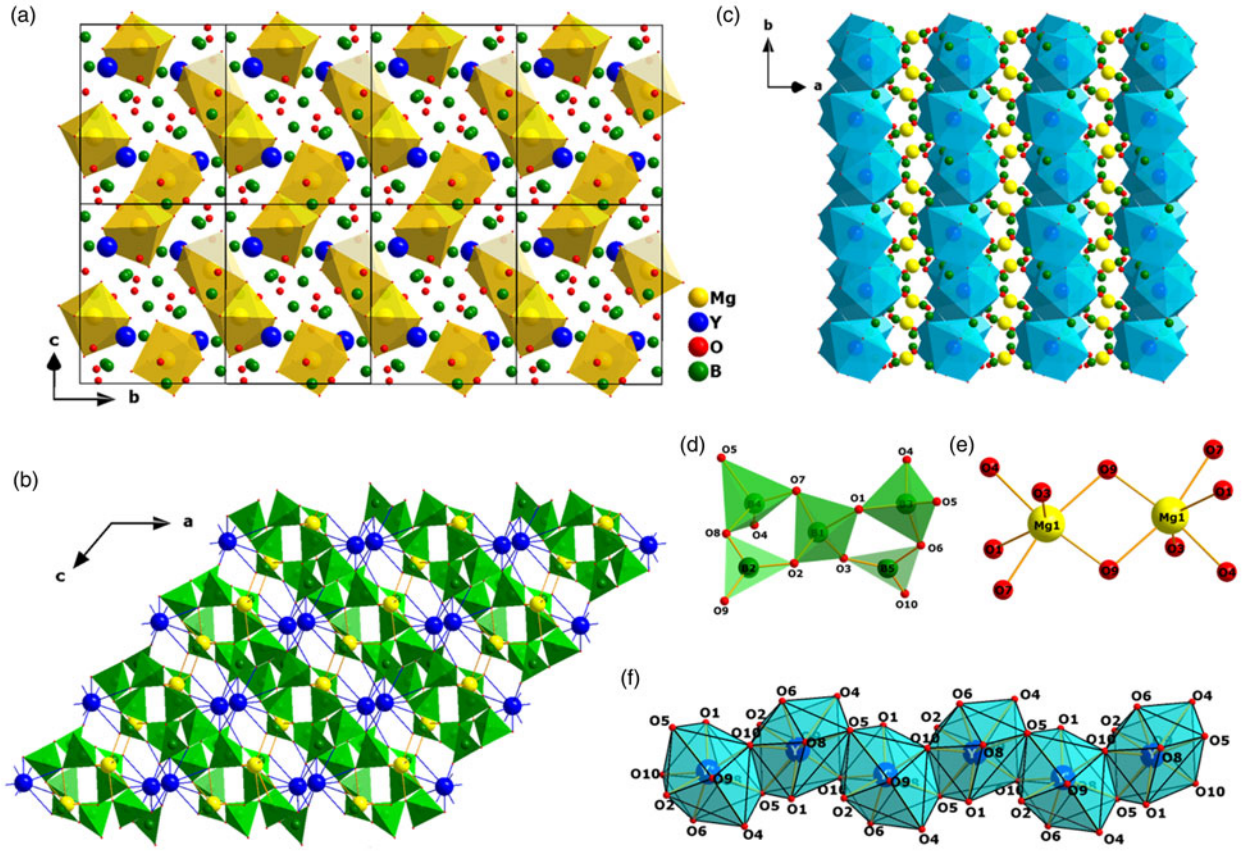

Figure 3. (a)–(c) The projection of $MgYB_5O_{10}$ along the [100], [010], and [001] directions, respectively. (d) Fundamental building block, B_5O_{12}, for the polyborate framework in $MgYB_5O_{10}$. (e) The isolated Mg_2O_{10} atom cluster formed by two adjacent MgO_6 groups through edge-sharing. (f) Infinite zigzag chains Y_nO_{8n+2} along the *b*-axis formed by edge-sharing YO_{10} polyhedra.

and two BO_3 triangles. However, in Cu*R*B_5O_{10} family, two tetrahedral BO_4 and two planar B_2O_5 groups are linked together, forming a 12-membered ring consisting of boron and oxygen, and the ring is connected with the next one via the BO_4 unit. The discrepancy of the anionic configuration and CN of *M* ions may be the main reason for the different space groups of *MR*B_5O_{10} family.

E. Diffuse reflectance spectra of $MgYB_5O_{10}$

Aimed at investigating the optical absorption characteristic in the UV–vis light region, UV–vis diffuse reflectance spectroscopy of pure $MgYB_5O_{10}$ was measured within the wavelength range of 190–700 nm. As can be seen in Figure 5(a), there exists a wide absorption band within 190–400 nm. For direct (or indirect) semiconductor, a figure can be plotted with $h\nu$ as the *x*-axis and $[F(R\infty)h\nu]^2$ (or $[F(R\infty)h\nu]^{0.5}$) as the *y*-axis, where $h\nu$ is equal to $1240/\lambda$ and $F(R\infty)$ is calculated from Kubelka–Munk function (López and Ricardo, 2012):

$$F(R\infty) = \frac{(1 - R\infty)}{2R\infty},$$

where $R\infty = 0.1^A$, and *A* is the absorption intensity.

The value at the intersection of the *x*-axis and extension of the straight portion is the optical band gap. Figures 5(b) and 5(c) show the extrapolation of direct and indirect band gaps E_{opt} for $MgYB_5O_{10}$ obtained from diffuse reflectance spectra, which are about 3.29 and 6.41 eV, respectively. The direct E_{opt} value 3.29 eV (~377 nm) fits well with the absorption edge of this material at about 400 nm. Since the host lattice is supposed to absorb VUV–UV excitement energy and transferred to luminescence center, the compound with large band gap is likely to have good luminescent properties after doping rare-earth ions. From this point of view, we can deduce that $MgYB_5O_{10}$ should have potential application value as a luminescent host material. As a matter of fact, there have been some previous researches about luminescent properties of active ions doped $MgYB_5O_{10}$. According to Ding's study, Tb^{3+} exhibits efficient emission in the Ce, Tb-codoped $MgYB_5O_{10}$ under the excitation of 365 nm (Ding, 1989). Besides, Eu^{3+}-doped $MgYB_5O_{10}$ has excitation band about 160 nm (in the VUV area), which promotes this compound to possess considerable application in the PDP (Plasma Display Panel) field (Wang and Wang, 2004).

F. Band structure (BS) of $MgYB_5O_{10}$

In order to better understand its basic physical properties, the BS of $MgYB_5O_{10}$ was calculated, and the result is presented in Figure 6. It possesses an indirect energy band gap of about 5.95 eV determined by A point at maximum of valence bands (VBM) and Γ point at minimum of conduction band (CBM). However, the real band gap for $MgYB_5O_{10}$ may

https://doi.org/10.1017/S0885715617000227 Published online by Cambridge University Press

TABLE V. Selected interatomic distances (Å), angles (°), and CN in structure $MgYB_5O_{10}$.

Mg	–O(1)	2.297(2)		–O(7)	1.425(2)
CN = 6	–O(3)	2.089(3)	⟨B(1)–O⟩ = 1.48 Å		
	–O(4)	2.151(2)	B(2)	–O(2)	1.316(1)
	–O(7)	2.032(2)	CN = 3	–O(8)	1.394(2)
	–O(9)	1.987(3)		–O(9)	1.354(2)
	–O(9)	2.101(2)	⟨B(2)–O⟩ = 1.35 Å		
⟨Mg–O⟩ = 2.11 Å			B(3)	–O(1)	1.455(2)
Y	–O(1)	2.415(2)	CN = 4	–O(4)	1.455(2)
CN = 10	–O(2)	2.484(1)		–O(5)	1.505(2)
	–O(4)	2.890(2)		–O(6)	1.458(2)
	–O(5)	2.524(2)	⟨B(3)–O⟩ = 1.47 Å		
	–O(5)	2.710(1)	B(4)	–O(4)	1.466(3)
	–O(6)	2.407(2)	CN = 4	–O(5)	1.618(1)
	–O(8)	2.757(1)		–O(7)	1.358(2)
	–O(9)	2.474(1)		–O(8)	1.512(2)
	–O(10)	2.291(1)	⟨B(4)–O⟩ = 1.49 Å		
	–O(10)	2.357(1)	B(5)	–O(3)	1.297(1)
⟨Y–O⟩ = 2.53 Å			CN = 3	–O(6)	1.388(2)
B(1)	–O(1)	1.599(2)		–O(10)	1.374(2)
CN = 4	–O(2)	1.385(2)	⟨B(5)–O⟩ = 1.35 Å		
	–O(3)	1.513(2)			
O(1)–B(1)–O(2)		108.0(1)	O(4)–B(3)–O(5)		111.2(1)
O(1)–B(1)–O(3)		103.5(1)	O(4)–B(3)–O(6)		116.0(1)
O(1)–B(1)–O(7)		99.7(1)	O(5)–B(3)–O(6)		106.1(1)
O(2)–B(1)–O(3)		110.6(1)	O(4)–B(4)–O(5)		106.9(1)
O(2)–B(1)–O(7)		121.5(1)	O(4)–B(4)–O(7)		117.0(1)
O(3)–B(1)–O(7)		111.3(1)	O(4)–B(4)–O(8)		109.0(1)
O(2)–B(2)–O(8)		116.0(1)	O(5)–B(4)–O(7)		109.2(1)
O(2)–B(2)–O(9)		122.2(1)	O(5)–B(4)–O(8)		100.2(1)
O(8)–B(2)–O(9)		121.7(1)	O(7)–B(4)–O(8)		113.0(1)
O(1)–B(3)–O(4)		106.4(1)	O(3)–B(5)–O(6)		122.7(1)
O(1)–B(3)–O(5)		105.7(1)	O(3)–B(5)–O(10)		120.2(1)
O(1)–B(3)–O(6)		111.1(1)	O(6)–B(5)–O(10)		115.6(1)

be a little different because GGA generally underestimates band gap of the 3*d* compound and some defects exit in real crystals. Interestingly, the result of first-principles calculations is corresponding to the deduced $E_{opt} = 6.41$ eV from its diffuse reflectance spectra by using the indirect method. Moreover, as can be seen from Figure 6, the valence band (VB) maximum is a flat band and the maximum values at point Γ and A in Briliouin zone is quite close, in which small disturbance (such as vacancy defects) may result in the transition from indirect band gap to direct band gap (Wei *et al.*, 2013; Ghosh and Gupta, 2015). Notably, the measured diffuse reflectance spectra and its deduced two type band-gap values are meaningful and acceptable. The possible explanation for the transition from indirect band gap to direct band gap is the existence of point defects in real crystal, whereas the model for the first-principles calculations is an ideal crystal without any defect.

In fact, a number of patents related to phosphors emitting UV radiation when stimulated by VUV radiation based on $MgYB_5O_{10}$ have been delivered previously, such as $YMgB_5O_{10}$: Gd, Ce (US Patent Nos. 4319161 and 6007741), and $YMgB_5O_{10}$: Gd, Ce, Pr (US Patent No. 7419621).

According to the calculated total density of states (TDOS) [Figure 7(a)] and partial density of states (PDOS) [Figure 7 (b)], the electronic structure in energy range from −25.0 eV to EF mainly comprises Y-*s* and O-*s*/p states with small contributions from B-*s*/*p* and Mg-*s*/*d*/*p* states. The significant contribution to the lower conduction band (CB) comes from

TABLE VI. Bond valence analysis of $MgYB_5O_{10}$.

Atoms	O(1)	O(2)	O(3)	O(4)	O(5)	O(6)	O(7)	O(8)	O(9)	O(10)	$\sum s_{calc}$	$\sum s_{theo}$
Mg(1)	0.1953*1		0.3426*1	0.2899*1			0.3998*1		0.4514*1		2.0108	2
									0.3318*1			
Y(1)	0.3427*1	0.2845*1		0.0949*1	0.2553*1	0.3502*1		0.1360*1	0.2923*1	0.4793*1	2.7908	3
					0.1545*1					0.4010*1		
B(1)	0.5407*1	0.9642*1	0.6816*1					0.8637*1			3.0503	3
B(2)		1.1603						0.9395*1	1.0470*1		3.1468	3
B(3)	0.7967*1			0.7978*1	0.6967*1	0.7898*1					3.0810	3
B(4)				0.7744	0.5130		1.0358*1	0.6824*1			3.0055	3
B(5)			1.2201*1			0.9564*1			0.9922*1		3.1687	3
$\sum s_{calc}$	1.8756	2.4087	2.2449	1.9573	1.6196	2.0965	2.3000	1.7581	2.1234	1.8725		
$\sum s_{theo}$	2	2	2	2	2	2	2	2	2	2		

Note. The results refer to the equations $s = \exp[(r_0 - r)/B]$ with $r_0 = 1.693$ Å, 2.019 Å and 1.371 Å for Mg—O, Y–O, and B–O, respectively, and $B = 0.37$.

https://doi.org/10.1017/S0885715617000227 Published online by Cambridge University Press

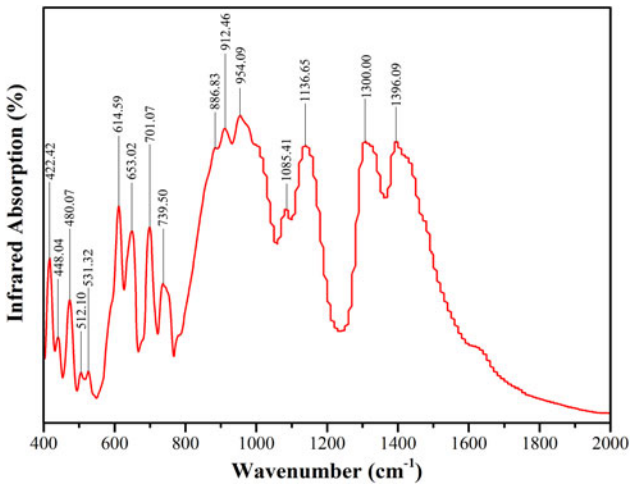

Figure 4. IR spectra for powder $MgYB_5O_{10}$ sample.

TABLE VII. IR band positions (cm^{-1}) of $MgYB_5O_{10}$ and $Na_3ZnB_5O_{10}$ (Chen *et al.*, 2012).

$MgYB_5O_{10}$	$Na_3ZnB_5O_{10}$	Assignment
1300–1500	1200–1480	ν_{as} of BO_3
1000–1200	~1028	ν_{as} of BO_4
800–1000	~940	ν_s of BO_3
680–800	~777	ν_s of BO_4 groups and γ of BO_3 groups
<680	<723	γ and δ of BO_3 and BO_4 groups

the Y-*d* state. It is obvious that the Y-*d* and Mg-*s*/*p* states in CB have a dominant effect on the energy band gap dispersion, while the O-*s*, B-*s*/*p* and Mg-*p*/*d* states in the upper VB have considerable effect on the dispersion. The PDOS of $MgYB_5O_{10}$ shows that Mg-*p*/*d* and B-*p* hybridize with O-*p* state at the VBM, and that Y-*d* and Mg/B-*p* hybridize with O-*p* state at the CBM. In addition, these results show that electrons, transferred from O-*p*, B-*p*, Mg-*p*/*d*, and Y-*p*/*d* states into VB, can contribute to weak covalence interactions of Mg–O and Y–O atom pairs as well as the substantial covalence interactions of B and O atoms.

IV. CONCLUSIONS

In this work, sub-solidus phase relations of the MgO–Y_2O_3–B_2O_3 ternary system were determined. One pentaborate with the composition $MgYB_5O_{10}$ has been synthesized and its crystal structure has been investigated. Based on the structure model of $ZnLaB_5O_{10}$, the Rietveld method was utilized to refine the parameters of the $MgYB_5O_{10}$ from powder XRD data. The crystal structure of $MgYB_5O_{10}$ is composed of MgO_6 octahedra, YO_{10} polyhedra, triangular BO_3, and tetrahedral BO_4 groups. The framework can be regarded as infinite 2D layers $[B_5O_{10}]_n^{5-}$ linked together by Mg and Y atoms. The IR spectra of $MgYB_5O_{10}$ at room temperature verified the existence of BO_3 and BO_4. Diffuse reflectance spectra of $MgYB_5O_{10}$ shows wide absorption in the range of 190–400 nm, which indicates the compound may be a promising luminescence host materials. Most of the pentaborate family

TABLE VIII. Crystal information of compounds MRB_5O_{10} (*M* and *R* are divalent and trivalent cations, respectively).

Compound	Space group	CN (*M*)	CN (*R*)	*a* (Å)	*b* (Å)	*c* (Å)	*β* (°)	*V* (Å^3)	Ref
$MgYB_5O_{10}$	$P12_1/c1$	6	10	8.511	7.589	12.246	130.200	604.2	This work
$MgLaB_5O_{10}$	$P12_1/c1$	6	10	8.807	7.611	12.731	131.520	638.9	Saubat *et al.* (1980)
$MgCeB_5O_{10}$	$P12_1/c1$	6	10	8.798	7.612	12.653	131.500	634.6	Saubat *et al.* (1980)
$MgPrB_5O_{10}$	$P12_1/c1$	6	10	8.765	7.574	12.591	131.420	626.8	Saubat *et al.* (1980)
$MgNdB_5O_{10}$	$P12_1/c1$	6	10	8.755	7.549	12.569	131.400	623.1	Saubat *et al.* (1980)
$MgSmB_5O_{10}$	$P12_1/c1$	6	10	8.723	7.511	12.492	131.250	615.3	Saubat *et al.* (1980)
$MgEuB_5O_{10}$	$P12_1/c1$	6	10	8.710	7.511	12.500	131.220	615.1	Saubat *et al.* (1980)
$MgGdB_5O_{10}$	$P12_1/c1$	6	10	8.697	7.480	12.451	131.170	609.7	Fan *et al.* (2006)
$MgTbB_5O_{10}$	$P12_1/c1$	6	10	8.683	7.455	12.394	131.040	605.1	Saubat *et al.* (1980)
$MgDyB_5O_{10}$	$P12_1/c1$	6	10	8.674	7.449	12.387	130.900	605.0	Saubat *et al.* (1980)
$MgHoB_5O_{10}$	$P12_1/c1$	6	10	8.654	7.424	12.366	130.820	601.2	Saubat *et al.* (1980)
$MgErB_5O_{10}$	$P12_1/c1$	6	10	8.611	7.400	12.317	130.660	595.4	Saubat *et al.* (1980)
$ZnLaB_5O_{10}$	$P12_1/c1$	6	9	8.792	7.629	12.688	131.138	641.0	Jiao *et al.* (2010)
$ZnCeB_5O_{10}$	$P12_1/c1$	6	10	8.745	7.614	12.594	131.112	631.8	Busche and Bluhm (1996)
$ZnNdB_5O_{10}$	$P12_1/c1$	6	10	8.686	7.609	12.505	130.932	624.4	Busche and Bluhm (1996)
$ZnTbB_5O_{10}$	$P12_1/c1$	6	10	8.582	7.605	12.324	130.471	611.9	Busche and Bluhm (1996)
$NiNdB_5O_{10}$	$P12_1/c1$	6	10	8.617	7.565	12.415	130.396	616.3	Campa *et al.* (1995)
$NiGdB_5O_{10}$	$P12_1/c1$	6	10	8.514	7.554	12.287	139.930	606.0	Campa *et al.* (1995)
$CdLaB_5O_{10}$	$P12_1/c1$	6	10	8.765	7.884	12.962	131.474	666.0	Wiesch and Bluhm (1997)
$CdSmB_5O_{10}$	$P12_1/c1$	6	10	8.588	7.882	12.604	130.565	648.1	Wiesch and Bluhm (1997)
$CdEuB_5O_{10}$	$P12_1/c1$	6	10	8.548	7.881	12.554	130.329	644.7	Wiesch and Bluhm (1997)
$CoYB_5O_{10}$	$P12_1/c1$	6	10	8.514	7.602	12.251	130.05	607.0	Campa *et al.* (1995)
$CoLaB_5O_{10}$	$P12_1/c1$	6	10	8.85	7.63	12.871	131.405	651.9	Abdullaev *et al.* (1975a)
$CoGdB_5O_{10}$	$P12_1/c1$	6	10	8.560	7.578	12.317	130.583	606.8	Campa *et al.* (1995)
$CoSmB_5O_{10}$	$P12_1/c1$	6	9	8.610	7.580	12.560	131.243	616.4	Abdullaev *et al.* (1975b)
$CoHoB_5O_{10}$	$P12_1/c1$	6	10	8.502	7.580	12.232	130.047	603.5	Алиев (2007)
$CoNdB_5O_{10}$	$P12_1/c1$	6	10	8.65	7.61	12.55	131.012	623.4	Abdullaev (1976)
$CoYbB_5O_{10}$	$P12_1/c1$	6	10	8.529	7.607	12.267	130.021	609.5	Алиев (2007)
$CuTmB_5O_{10}$	*Iba*2	6	8	6.220	8.447	12.663	90	665.3	Schaefer and Bluhm (1995b)
$CuTbB_5O_{10}$	*Iba*2	6	8	6.294	8.406	12.733	90	673.7	Schaefer and Bluhm (1995a)
$CuLuB_5O_{10}$	*Iba*2	6	8	6.184	8.458	12.609	90	659.5	Schaefer and Bluhm (1995b)

https://doi.org/10.1017/S0885715617000227 Published online by Cambridge University Press

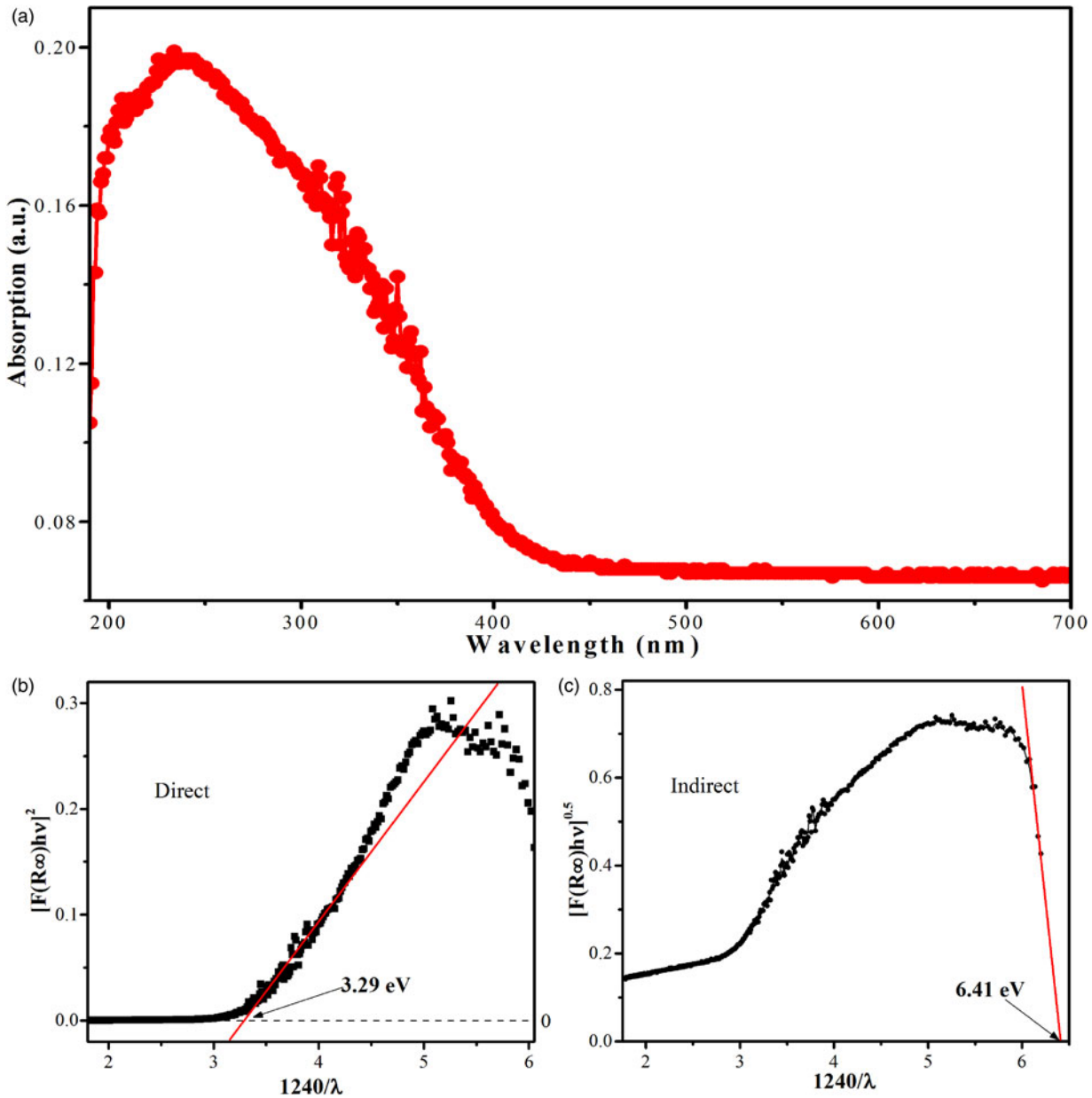

Figure 5. (a) The UV–vis diffuse reflectance spectra of $MgYB_5O_{10}$ at room temperature. The extrapolation of direct and indirect band gaps for $MgYB_5O_{10}$ is illustrated in (b) and (c).

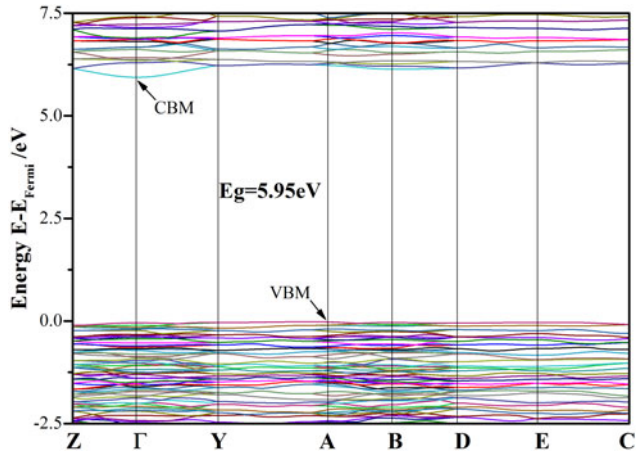

Figure 6. The calculated BSs of $MgYB_5O_{10}$.

MRB_5O_{10} (M and R are divalent and trivalent cations, respectively) crystallize in the $P12_1/c1$ (No. 14) space group, whereas those compounds containing copper $CuRB_5O_{10}$ are in $Iba2$ (No. 45). This may be because of the discrepancy of the anionic configuration and CN of M ions. The optical band gap of $MgYB_5O_{10}$ was determined from the UV–vis diffuse reflectance spectra by Kubelka–Munk function. The first-principles calculations of its electronic structure reveal that $MgYB_5O_{10}$ is an insulator with an indirect energy of about 5.95 eV, which is near to the indirect band gap value extrapolated from diffuse reflectance spectra. Meanwhile, the measured absorption edge is in agreement with deduced direct band gap according to diffuse reflectance spectra. Angular momentum characters of each structure groups in its electronic structure were identified according to the PDOS. The nature of chemical bonding in this structure has been elucidated from its

https://doi.org/10.1017/S0885715617000227 Published online by Cambridge University Press

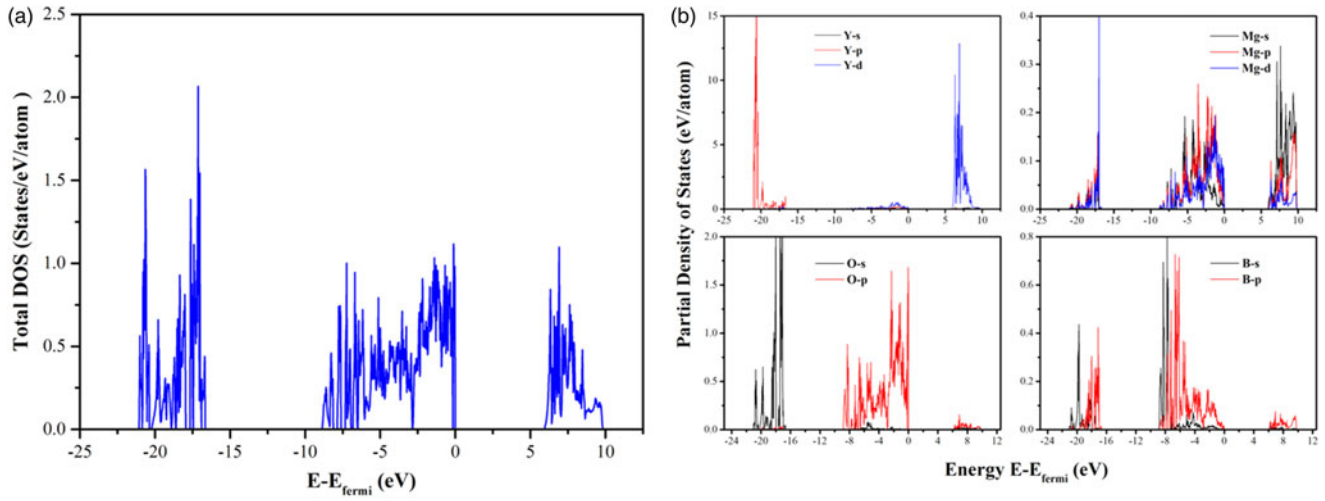

Figure 7. (a) The calculated TDOS of $MgYB_5O_{10}$. (b) The calculated PDOS of $MgYB_5O_{10}$.

TDOS and PDOS. The structural characteristics of both crystalline and electronic might make $MgYB_5O_{10}$ an excellent host for phosphors and a superior material for UV applications.

SUPPLEMENTARY MATERIAL

The supplementary material for this article can be found at https://doi.org/10.1017/S0885715617000227

ACKNOWLEDGEMENTS

Financial supports by the National Natural Science Foundation of China (Grant number 51472273) and Major State Basic Research Development Program of China (Grant number 2014CB6644002) are gratefully acknowledged. The work was also supported through a Grant-in-Aid from Department for Science and Technology of Hunan province (Grant number 2014FJ4099), the Projects of Innovation-driven Plan in Central South University (Grant number 2015CX004) and State Key Laboratory of Powder Metallurgy (Central South University, Changsha, China).

Abdullaev, G. K. (**1976**). "Crystal structure of the double metaborate of neodymium and cobalt $NdCo(BO_2)_5$," J. Struct. Chem. **17**, 961–963.

Abdullaev, G. K., Mamedov, K. S., and Dzhafarov, G. G. (**1975a**). "Crystal structure of $LaCo(BO_2)_5$," J. Struct. Chem. **16**, 61–65.

Abdullaev, G. K., Mamedov, K. S., and Dzhafarov, G. G. (**1975b**). "Crystal structure of the double metaborate of samarium and cobalt $SmCo(BO_2)_5$," Sov. Phys. Crystallogr. **19**, 457–459.

Алиев, О. А. (**2007**). "Двойные метабораты редкоземельных элементов и кобальта состава $LnCo(BO_2)_5$," Известия высших учебных заведений. Химия и химическая технология **50**, 44–47.

Bartl, H. and Schuckmann, W. (**1966**). "Zur Struktur des Magnesiumdiborates, $MgO \cdot 2B_3O_2$," NeuesJahrb. Miner. Monatsh. **1966**, 142–148.

Bazarova, Z. G., Nepomnyashchikh, A. I., Kozlov, A. A., Bogdan-Kurilo, V. D., Bazarov, B. G., Subanakov, A. K., and Kurbatov, R. V. (**2007**). "Phase equilibria in the system Li_2O–MgO–B_2O_3," Russ. J. Inorg. Chem. **52**, 1971–1973.

Becker, P. (**1998**). "Borate materials in nonlinear optics," Adv. Mater. **10**, 979–992.

Bosenberg, W. R., Pelouch, W. S., and Tang, C. L. (**1989**). "High-efficiency and narrow-linewidth operation of a two-crystal β-BaB_2O_4 optical parametric oscillator," Appl. Phys. Lett. **55**, 1952–1954.

Boultif, A. and Louër, D. (**2004**). "Powder pattern indexing with the dichotomy method," J. Appl. Crystallogr. **37**, 724–731.

Brown, I. D. and Altermatt, D. (**1985**). "Bond-valence parameters obtained from a systematic analysis of the Inorganic Crystal Structure Database," Acta Crystallogr. **B41**, 244–247.

Busche, S. and Bluhm, K. (**1996**). "Synthesis and crystal structure of rare earth zinc borates $LnZn(B_5O_{10})$ with *Ln*= Ce, Nd, Tb," Z. Naturforsch. B **51**, 671–676.

Cai, G. M., Chen, X. L., Wang, W. Y., Lou, Y. F., Liu, J., Zhao, J. T., and Chen, H. H. (**2008**). "A new promising scintillator $Ba_3InB_9O_{18}$," J. Solid State Chem. **181**, 646–651.

Campa, J. A., Cascales, C., Puebla, E. G., Mira, J., Monge, M. A., Rasines, I., Rivas, I., and Valero, C. R. (**1995**). "Crystal structure and magnetic properties of $CoR(BO_2)_5$ (*R* = Y, Gd) and $NiR(BO_2)_5$ (*R* = Nd, Gd)," J. Alloy. Compd. **225**, 225–229.

Chadeyron, G., El-Ghozzi, M., Mahiou, R., Arbus, A., and Cousseins, J. C. (**1997**). "Revised structure of the orthoborate YBO_3," J. Solid State Chem. **128**, 261–266.

Chen, C. T., Wu, Y. C., and Li, R. K. (**1990**). "The development of new NLO crystals in the borate series," J. Cryst. Growth **99**, 790–798.

Chen, S. J., Pan, S. L., Wu, H. P., Han, J., Zhang, M., and Zhang, F. F. (**2012**). "Synthesis, crystal structure and optical properties of a new orthorhombic phase, $Na_3ZnB_5O_{10}$," J. Mol. Struct. **1021**, 118–122.

Chen, X., Li, M., Zuo, J., Chang, X., Zang, H., and Xiao, W. (**2007**). "Syntheses and crystal structures of two pentaborates, $Na_3CaB_5O_{10}$ and $Na_3MgB_5O_{10}$," Solid State Sci. **9**, 678–685.

Ding, X. (**1989**). "Luminescence and excitation spectra of Ce^{3+}-Tb^{3+} ions co-doped in the $LnMgB_5O_{10}$ system," J. Less Common Met. **148**, 393–397.

Fan, J. M., Lin, Z. B., Zhang, L. Z., and Wang, G. F. (**2006**). "Structure of $GdMg(BO_2)_5$ crystal," Chin. J. Struct. Chem. **25**, 709–713.

Fletcher, B. L., Stevenson, J. R., and Whitaker, A. (**1970**). "Phase equilibria in the system CaO-MgO-B_2O_3 at 900 °C," J. Am. Ceram. Soc. **53**, 95–97.

Ghosh, B. and Gupta, A. (**2015**). "Effect of defects on the electronic properties of WS_2 armchair nanoribbon," J. Semicond. **36**, 0130031–0130034.

Guo, G. C., Cheng, W. D., Chen, J. T., Huang, J. S., and Zhang, Q. E. (**1995**). "Triclinic $Mg_2B_2O_5$," Acta Crystallogr. **C51**, 351–353.

Hong, G. Y. (**2011**). *Rare Earth luminescent Materials: Fundamentals and Applications* (Science Press, Beijing). (in Chinese).

Hu, Z. G., Higashiyama, T., Yoshimura, M., Yap, Y. K., Mori, Y., and Sasaki, T. (**1998**). "A new nonlinear optical borate crystal $K_2Al_2B_2O_7$ (KAB)," Jpn. J. Appl. Phys. **37**, 10A.

Hu, Q., Wang, L., Huang, Z., and Fang, Z. (**2015**). "Tunable single-phase white-light-emitting $Ba_2Mg(BO_3)_2$: Ce^{3+}, Na^+, Tb^{3+}, Eu^{2+} phosphor based on energy transfer," Ceram. Int. **41**, 8988–8995.

Jiang, X. X., Molokeev, M. S., Gong, P. F., Yang, Y., Wang, W., Wang, S. H., Wu, S. F., Wang, Y. X., Huang, R. J., Li, L. F., Wu, Y. C., Xing, X. R., and Lin, Z. S. (**2016**). "Near-zero thermal expansion and high ultraviolet transparency in a borate crystal of $Zn_4B_6O_{13}$," Adv. Mater. **28**, 7936–7940.

Jiao, Z. W., Wang, R. J., Wang, X. Q., Shen, D. Z., and Shen, G. Q. (**2010**). "$LaZnB_5O_{10}$, the first lanthanum zinc borate," Acta Crystallogr. **E66**, i1.

Kellner, T., Heine, F., and Huber, G. (**1997**). "Efficient laser performance of Nd:YAG at 946 nm and intracavity frequency doubling with $LiIO_3$, β-BaB_2O_4, and LiB_3O_5," Appl. Phys. B **65**, 789–792.

Knitel, M. J., Dorenbos, P., and Van Eijk, C. W. E. (**2000**). "Photoluminescence, and scintillation/thermoluminescence yields of several Ce^{3+} and Eu^{2+} activated borates," Nucl. Instrum. Methods A **443**, 364–374.

Kong, F., Huang, S. P., Sun, Z. M., Mao, J. G., and Cheng, W. D. (**2006**). "$Se_2(B_2O_7)$: a new type of second-order NLO material," J. Am. Chem. Soc. **128**, 7750–7751.

Kuzel, H. J. (**1964**). "Investigation of the MgO-B_2O_3 system: synthesis and x-ray study of the compound $MgO \cdot 2B_2O_3$," Neues Jahrb. Mineral. Monatsh. **12**, 357–360.

Levin, E. M., Roth, R. S., and Martin, J. B. (**1961**). "Polymorphism of ABO_3 type rare earth borates," Am. Mineral. **46**, 1030–1055.

Li, X. Z., Chen, X. L., Wu, L., Cao, Y. G., Zhou, T., and Xu, Y. P. (**2004**). "$Ba_3YB_3O_9$: phase transition and crystal structure," J. Alloy Compd. **370**, 53–58.

Li, H. K., Cai, G. M., Fan, J. J., Jin, Z. P., Zhou, T. T., and Chen, X. L. (**2013**). "Crystal structures of two novel borate compounds $MgInBO_4$ and $MgIn_{7/8}B_{7/8}O_{29/8}$," J. Solid State Chem. **202**, 262–268.

Lou, Y. F., Li, D. D., Li, Z. L., Zhang, H., Jin, S. F., and Chen, X. L. (**2015**). "Unidirectional thermal expansion in edge-sharing BO_4 tetrahedra contained $KZnB_3O_6$," Sci. Rep. **5**, 10996.

López, R. and Ricardo, G. (**2012**). "Band-gap energy estimation from diffuse reflectance measurements on sol–gel and commercial TiO_2: a comparative study," J. Sol-gel Sci. Technol. **61**, 1–7.

Mutluer, T. and Timucin, M. (**1975**). "Phase equilibria in the system MgO–B_2O_3," J. Am. Ceram. Soc. **58**, 196–197.

Peterson, G. A. (**1999**). *Studies on New Inorganic Solid-State Borates and Oxoanion Fluorides* (Oregon State University, Oregon, Corvallis).

Rietveld, H. M. (**1967**). "Line profiles of neutron powder-diffraction peaks for structure refinement," Acta Crystallogr. **22**, 151–152.

Sadanaga, R. (**1948**). "The crystal structure of kotoite $Mg_3B_2O_6$," X-Rays **5**, 2–7.

Sasaki, T., Mori, Y., Yoshimura, M., Yap, Y. K., and Kamimura, T. (**2000**). "Recent development of nonlinear optical borate crystals: key materials for generation of visible and UV light," Mater. Sci. Eng. R: Rep. **30**, 1–54.

Saubat, B., Vlasse, M., and Fouassier, C. (**1980**). "Synthesis and structural study of the new rare earth magnesium borates $LnMgB_5O_{10}$ (Ln = La,. . ., Er)," J. Solid State Chem. **34**, 271–277.

Schaefer, J. and Bluhm, K. (**1995a**). "$CuTb[B_5O_{10}]$: Das erste "Metaborat" mit $^1_\infty[B_5O_{10}]^{5-}$ einem Anion," Z. Anorg. Allg. Chem. **621**, 567–570.

Schaefer, J. and Bluhm, K. (**1995b**). "Synthesis and crystal structure of compounds of the type $CuM[B_5O_{10}]$ (M = Tm^{3+}, Lu^{3+})," Z. Naturforsch. B **50**, 762–766.

Shi, Q., You, F., Huang, S., Cui, J., Huang, Y., and Tao, Y. (**2016**). "Host sensitization of Tb^{3+} through Gd^{3+} in $Na_3Gd(BO_3)_2$: Tb^{3+}," J. Alloy. Compd. **654**, 441–444.

Wang, L. L. and Wang, Y. H. (**2004**). "Relationships between structural and luminescence properties in europium doped borate under VUV excitation (in Chinese)," J. Chin. Rare Earth Soc. **22**, 863–866.

Wei, Z. G., Sun, L. D., Liao, C. S., Yan, C. H., and Huang, S. H. (**2002**). "Fluorescence intensity and color purity improvement in nanosized YBO_3: Eu," Appl. Phys. Lett. **80**, 1447–1449.

Wei, Z., Yuan, J. M., Li, S. H., Liao, J., and Mao, Y. L. (**2013**). "Density functional study on the electronic and magnetic properties of two-dimensional hexagonal boron nitride containing vacancy," Acta Phys. Sin. **62**, 2013101–2013107.

Wiesch, A. and Bluhm, K. (**1997**). "The first cadmium rare earth borates $CdLn[B_5O_{10}]$ with Ln = La, Sm, Eu," Acta Crystallogr. C: Cryst. Struct. Commun. **53**, 1730–1733.

Yang, Z., Chen, X. L., Liang, J. K., Lan, Y. C., and Xu, T. (**2001**). "Phase relations in the MgO-Ga_2O_3-B_2O_3 system and the crystal structure of $MgGaBO_4$," J. Alloy Compd. **319**, 247–252.

Yang, L., Wan, Y., Huang, Y., Chen, C., and Seo, H. J. (**2016**). "Development of $YK_3B_6O_{12}$: RE (RE = Eu^{3+}, Tb^{3+}, Ce^{3+}) tricolor phosphors under near-UV light excitation," J. Alloy. Compd. **684**, 40–46.

Ye, S., Li, Y. J., Yu, D. C., Dong, G. P., and Zhang, Q. Y. (**2011**). "Room-temperature upconverted white light from $GdMgB_5O_{10}$: Yb^{3+}, Mn^{2+}," J. Mater. Chem. **21**, 3735–3739.

Zhou, D., He, D. W., Liang, Z. Y., and Hou, T. (**2007**). "Luminescence properties of MO-Re_2O_3-B_2O_3: Eu^{3+} (M = Mg, Sr; Re = Y, Gd) under VUV excitation," Key Eng. Mater. **336**, 597–599.

https://doi.org/10.1017/S0885715617000227 Published online by Cambridge University Press